# III-3

## Chemistry

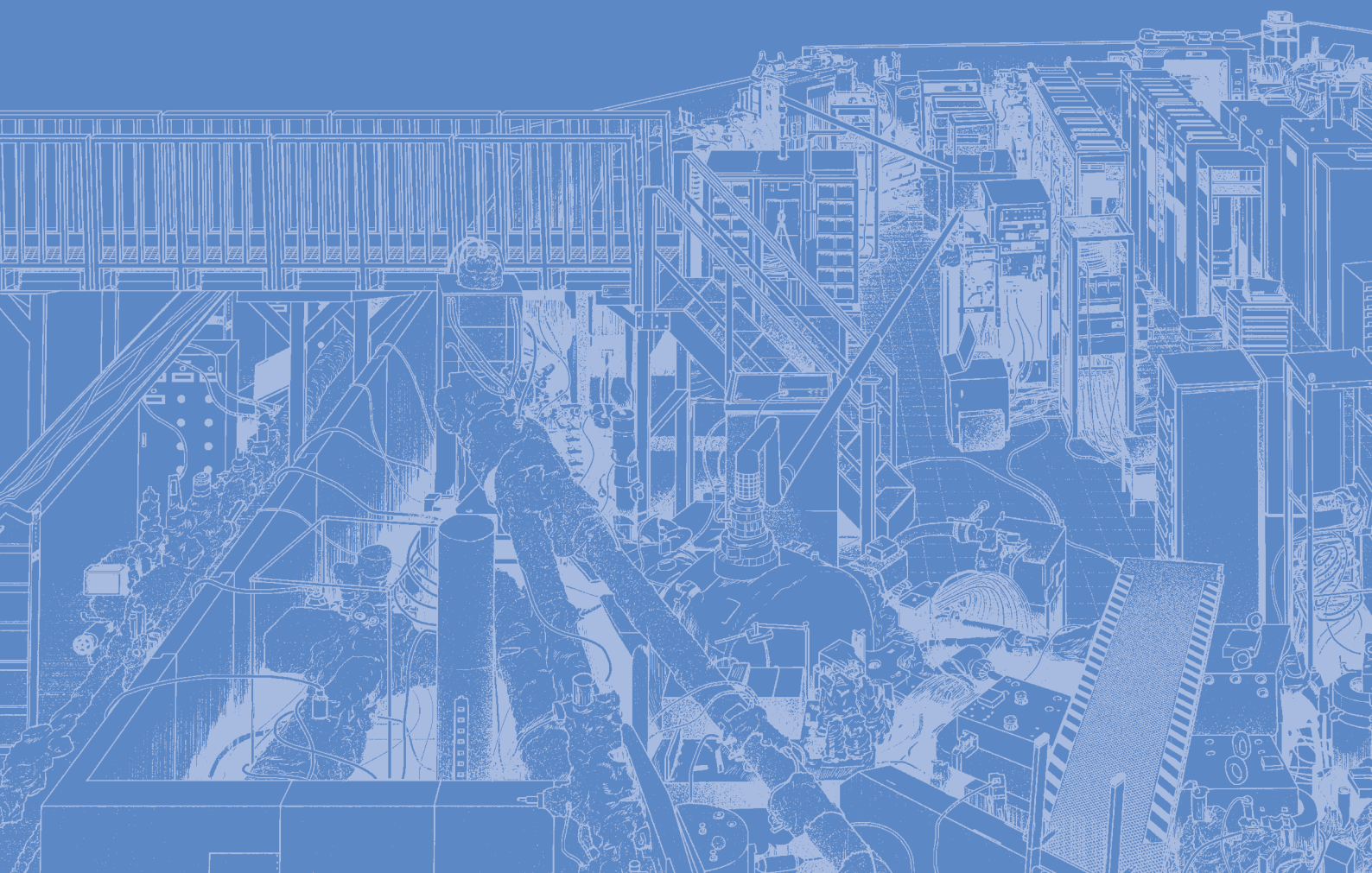

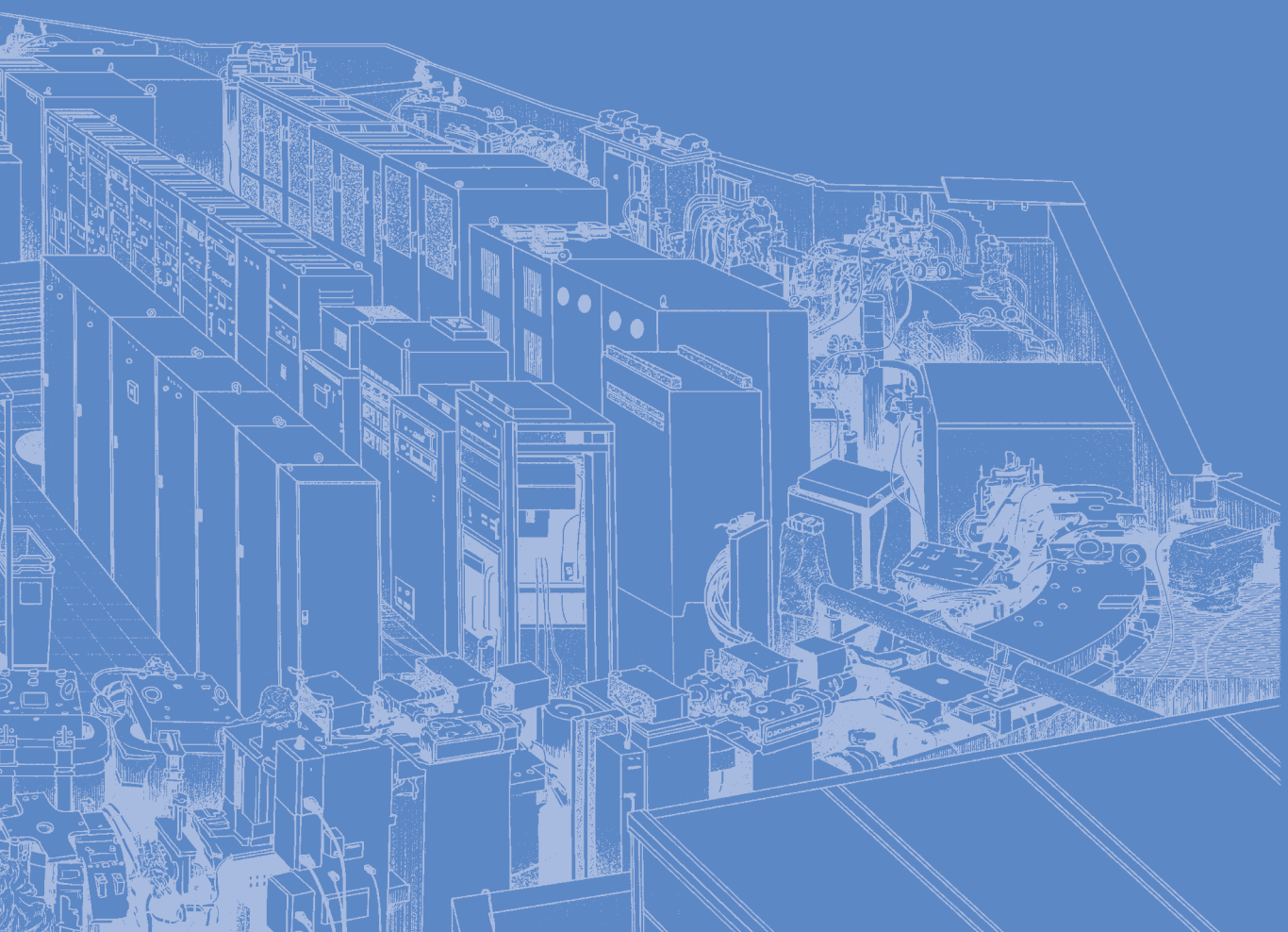

BL1U

# Search for Chiral Systems Exhibiting Novel Type of Photoelectron Circular Dichroism

H. Kohguchi[1], Y. Hikosaka[2], T. Kaneyasu[3], S. Wada[1], H. Ota[4], M. Katoh[1,4] and Y-I. Suzuki[5]

[1]*Graduate School of Advanced Science and Engineering, Hiroshima University, Higashi-Hiroshima 739-8526, Japan*

[2]*Institute of Liberal Arts and Sciences, University of Toyama, Toyama 930-0194, Japan*

[3]*SAGA Light Source, Tosu 841-0005, Japan*

[4]*UVSOR Synchrotron Facility, Institute for Molecular Science, Okazaki 444-8585, Japan*

[5]*School of Medical Technology, Health Sciences University of Hokkaido, Tobetsu 061-0293, Japan*

Photoelectron circular dichroism (PECD) is a sensitive probe for molecular chirality, which is one of the most attractive molecular properties in chemistry. The PECD parameter is defined as a $b_1$ coefficient associated with the first-order Legendre polynomial ($P_1(\cos\theta)$) in the difference photoelectron angular distributions between left- and right-handed circularly polarized ionization light. The BL1U beamline is highly suited for the PECD study since the undulator provides well-defined circularly polarized light in the vacuum ultraviolet region, where the $b_1$ parameter is generally maximized for most chiral molecules. The $b_1$ parameter exhibits particular photon energy dependence on the molecular species, for which we have developed our PECD study [1]. As well as the photoelectron kinetic energy dependence of the $b_1$ parameter, the state dependence of PECD is essential to determine the chirality of the relevant molecular orbitals. Thus, high-resolution photoelectron spectroscopy serves as a basis for a deep understanding of the PECD mechanism.

At the BL1U beamline, we measured the energy- and state-dependence of the PECD of methyl oxirane [2], a typical chiral molecule exhibiting PECD. Since the oxirane framework, where an asymmetric carbon atom is located, is more relevant to molecular chirality, we expected the PECD manifestation for other oxiranes.

We carried out the VMI measurements of several oxiranes at varied photon energies. The PECD results of methyl oxirane, well-known in previous studies, were used as a standard for optimizing the measurement condition. Examples of the results of the VMI measurements are shown in Fig. 1. The measurements with linearly polarized light (Fig. 1, upper) provide a basis for the state assignments. The photoelectron spectra obtained from the VMI data with linear polarization of phenyl oxirane were much different from those of methyl oxirane; the ionization threshold was lowered by approximately 2 eV, and the spectral peak structures in the vicinity of the threshold were not assignable to corresponding peaks of the methyl oxirane spectrum. We assumed that the photoionization relevant to the molecular orbitals associated with the oxirane framework should show a similar PECD to that of methyl oxirane. The result of the PECD measurements, however, exhibited no chiral property for phenyl oxirane (Fig. 1 lower). Apparently biased positive (red) and negative (blue) intensity found in the difference image data at 90 nm is not a signature of PECD but an experimental artifact because PECD should appear as an asymmetric distribution with respect to the circularly polarized radiation propagation (vertical direction in the images). The $b_1$ values at other photon energy were also negligibly small compared to the PECD intensity of methyl oxirane. Electronic modification by phenyl substitution was found to be so large that the photoelectron spectra, especially in the low kinetic energy photoelectron region, were heavily altered, and the chirality around the asymmetric carbon was almost lost. The result indicates that PECD is more sensitive to the molecular electronic chirality than the photoelectron spectroscopy.

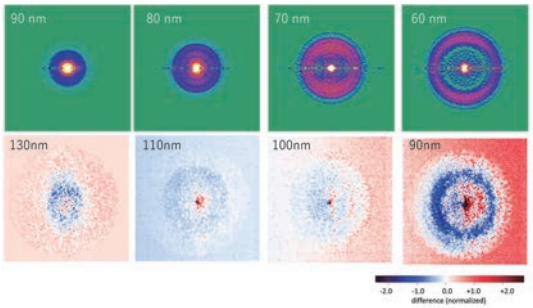


Fig. 1. Photoelectron scattering distributions of phenyl oxirane with linearly polarized light (upper) and circularly polarized light (lower) at several ionization wavelengths. The lower data are difference images between the right- and left-handedcircular polarizations.

[1] H. Kohguchi *et al.*, UVSOR Activity Report **50** (2023) 136.
[2] H. Kohguchi *et al.*, UVSOR Activity Report **49** (2021) 106.

BL1U

# Time-Domain Double Slit Interference of Electrons Produced by Light Wave Packets from a Tandem Undulator

T. Kaneyasu[1,2], Y. Hikosaka[3], S. Wada[4], M. Fujimoto[5], H. Ota[2], H. Iwayama[2,6] and M. Katoh[2,5,7]

[1]*SAGA Light Source, Tosu 841-0005, Japan*
[2]*Institute for Molecular Science, Okazaki 444-8585, Japan*
[3]*Institute of Liberal Arts and Sciences, University of Toyama, Toyama 930-0194, Japan*
[4]*Graduate School of Advanced Science and Engineering, Hiroshima University, Higashi-Hiroshima 739-8526, Japan*
[5]*Synchrotron Radiation Research Center, Nagoya University, Nagoya 464-8603, Japan*
[6]*SOKENDAI (The Graduate University for Advanced Studies), Okazaki 444-8585, Japan*
[7]*Hiroshima Synchrotron Radiation Center, Hiroshima University, Higashi-Hiroshima 739-0046, Japan*



Wave-particle duality is one of the most fundamental concepts in quantum mechanics. The concept has previously been beautifully demonstrated by the double-slit experiment, in which particles such as electrons, atoms, molecules and neutrons passing through the double-slit exhibit interference patterns in the intensity distribution on a detection screen. Since there is an analogy between spatial diffraction and temporal dispersion in optics, the observation of double-slit interference with particles is not restricted to conventional space-domain experiments but can be extended to time-domain experiments. In this study, we present a new realization of the time-domain double-slit experiment with photoelectrons, demonstrating that spontaneous radiation from a bunch of relativistic electrons can be used to control the quantum interference of single particles [1].

To produce the temporal double-slit, we use a tandem-undulator system in which each relativistic electron in the bunch emits a pair of light wave packets that has a mutual coherence between them [2,3]. A pair of light wave packets sequentially interacts with a helium atom, producing a pair of photoelectron wave packets that propagate in free space and overlap each other, leading to the appearance of the interference pattern. In order to visualize the buildup of the interference pattern, we observe the interference in the energy domain (Fig. 1).

We recorded photoelectron images using a two-dimensional (2D) position-sensitive detector mounted in a hemispherical electron energy analyzer. The 2D detector allows for one-by-one detection of the photoelectrons. Figure 2 compares the CCD images of photoelectrons recorded with the radiation from single- and tandem-undulator configurations. In both cases, the central wavelength of the undulator radiation was 43 nm. When the single undulator is used, the helium atom is ionized by light wave packets emitted from either the upstream or downstream undulator, leading to the production of single (not-paired) photoelectron wave packets. Therefore, no interference pattern can be exhibited on the CCD image. On the other hand, the buildup process of the quantum interference pattern is monitored by accumulating the CCD images when the radiation from the tandem undulator is used. The CCD image after accumulation of 2000 electrons shows an almost random distribution. An interference pattern exhibiting the wave-like nature of single photoelectrons appears at $2\times10^4$ electrons, and becomes clearer as the number of electrons is increased.

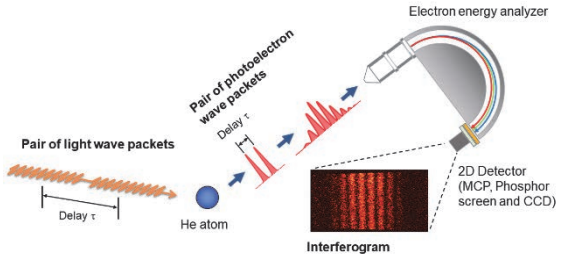


Fig. 1. Time-domain double-slit experiment using a tandem-undulator system.

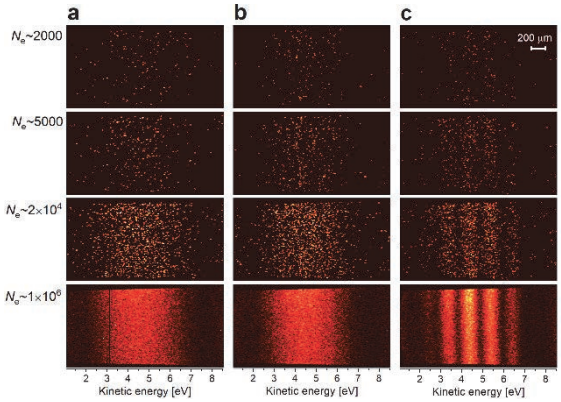


Fig. 2. CCD images of photoelectrons observed for radiation from (a) the upstream undulator, (b) the downstream undulator, and (c) the tandem undulator.

[1] T. Kaneyasu *et al*., Sci. Rep. **13** (2023) 6142.
[2] Y. Hikosaka *et al*., Nat. Commun. **10** (2019) 4988; **12** (2021) 3782.
[3] T. Kaneyasu *et al*., Sci. Rep. **12** (2022) 9682.

BL1U

# Measurement of Arbitrary Polarization by Zeeman Quantum Beat of Helium Atom

T. Kaneyasu[1,2], Y. Hikosaka[3], S. Wada[4], H. Kohguchi[4], M. Fujimoto[5], H. Ota[2], H. Iwayama[2,6], M. Hosaka[7] and M. Katoh[2,5,8]

[1]*SAGA Light Source, Tosu 841-0005, Japan*
[2]*Institute for Molecular Science, Okazaki 444-8585, Japan*
[3]*Institute of Liberal Arts and Sciences, University of Toyama, Toyama 930-0194, Japan*
[4]*Graduate School of Advanced Science and Engineering, Hiroshima University, Higashi-Hiroshima 739-8526, Japan*
[5]*Synchrotron Radiation Research Center, Nagoya University, Nagoya 464-8603, Japan*
[6]*SOKENDAI (The Graduate University for Advanced Studies), Okazaki 444-8585, Japan*
[7]*National Synchrotron Radiation Laboratory, University of Science and Technology of China, Hefei 230029, China*
[8]*Hiroshima Synchrotron Radiation Center, Hiroshima University, Higashi-Hiroshima 739-0046, Japan*

One of the unique capabilities of novel undulators used in modern synchrotrons is a polarization control. However, the actual polarization of light at the sample position often differs from the original one set by the undulator. This is mainly due to the reflection property of the beamline optics. To use the arbitrary polarization in the synchrotron radiation experiments, it is required to measure the actual polarization in a beamline.

We have recently developed a simple polarimetry method which uses a Zeeman quantum beat in the fluorescence decay of helium atoms [1,2]. In this study, we applied this method to investigate the actual polarization state of vacuum ultraviolet light at the beamline BL1U. The light source of BL1U is an APPLE-II type variably polarized undulator. The beamline consists of two toroidal mirrors and a Seya-Namioka monochromator. A small chamber equipped with two solenoid coils was set at the sample position to measure the Zeeman quantum beat of helium atoms. The photon energy was set to 24.2 eV to resonantly excite the 1s electron into the 6p orbital. We observed the fluorescence decay from the 1s6p into 1s2s state, emitting 345-nm wavelength photon. During the measurement, the UVSOR ring was operated in a single bunch mode, providing light pulses with a 178 ns period.

Figure 1 shows the fluorescence decay curves measured with different phases of the undulator magnets. The polarization state of undulator radiation smoothly changes from horizontal linear to elliptical and finally to vertical linear when the phase is changed. The fluorescence decay curves exhibit quantum beat oscillations superimposed on the exponential decay, reflecting the polarization state; the contrast and initial phase of the oscillations corresponds to the degree of linear polarization and the tilt angle of the polarization ellipse, respectively [2]. The beat structure almost vanishes at 21 mm phase, indicating that the degree of circular polarization is highest among the measurements, although one can expect that the undulator radiates almost fully circularly polarized light at 28.6 mm phase. The observed difference can be explained by the effect of beamline optics. The experimental curves are well reproduced by a simulation which takes into account the polarization state of the undulator radiation and reflection property of the beamline optics.

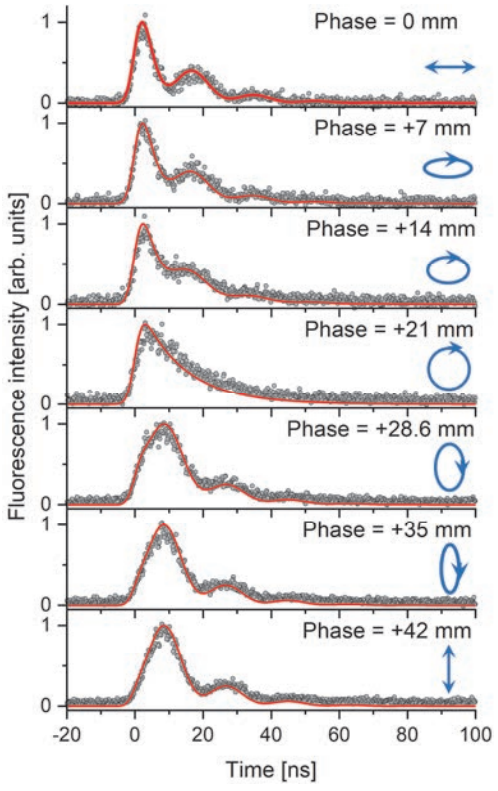


Fig. 1. Fluorescence decay curves of the 1s6p excited state of helium. The gray circles represent the experimental data while the red curve show the simulation results. Polarization ellipse assumed in the simulation is attached in each panel.

[1] Y. Hikosaka *et al*., J. Synchrotron Radiat. **27** (2020) 675.
[2] T. Kaneyasu *et al*., New J. Phys. **22** (2020) 083062.

BL3U

# Observation of the Electronic Structure of Aggregating Polymers in Shear Thickening Solutions

K. Akada[1,2], S. Sato[3], M. Kobayashi[4] and J. Fujita[1]

[1]*Institute of Applied Physics, Graduate School of Pure and Applied Sciences, University of Tsukuba, Tsukuba 305-8573, Japan*

[2]*Japan Synchrotron Radiation Research Institute (JASRI), SPring-8, Sayo-gun 679-5198, Japan*

[3]*Graduate School of Science and Technology, University of Tsukuba, Tsukuba 305-8572, Japan*

[4]*Faculty of Life and Environmental Sciences, University of Tsukuba, Tsukuba 305-8572, Japan*

A shear thickening fluid (STF) is a non-Newtonian fluid characterized by a significant increase in its viscosity when subject to a shear rate above a critical value. Some colloidal suspensions consisting of silica particles exhibit shear-thickening (ST) properties, which has a wide spectrum of potential applications in shock absorption, body protection, etc. Various works have been made so far to interpret the origins of the shear thickening mechanisms in various STF systems.

Among ST fluids, those composed of particles with a small diameter and a polymer solution, which gel upon impact, are called shake-gels (Fig. 1). Previous study said that a polymer network bridging particles reconstructs in response during gelation process, although the detailed mechanism is not well understood. One reason is the difficulty in measuring the ST state. The reconstructed network return to their original state once the shear stress is removed, making it difficult to measure the properties of the ST state.

Previous studies on the dynamics in the STF have mostly focused on bulk states that measure the viscosity of the entire solution or macroscopic measurements using particles larger than >μm. Few reports focusing on the clustering of smaller particles or the aggregation structure of water molecules and polymers.

Regarding the structure of nm particles, our previous studies have revealed that several hundred nm of the floc structures are formed with an increase in viscosity by measuring the structure under shear. This gelation occurs even when ST sample is flowing in a tube, and the ST phenomena can be controlled by flow rate and tube diameter.

By using X-ray Absorption Spectroscopy (XAS) at BL3U to measure the ST samples, we expected to obtain insights into polymer aggregation. The purpose of this study is understanding the polymer aggregation mechanism by measuring the dehydration of polymers with altered network structure and the changes in coordination and electronic states upon stretching.

As ST samples, suspensions of amorphous silica particles and PEG solution were prepared. The suspension consisted of silica particles with a diameter of 30 nm and PEG solutions with molecular weights of 1000 kDa. A flow cell was used for H2O and silica dispersion. In cases of measuring high viscosity sample, the flow paths could become jammed, and sealed cell was adopted.

Figure 2 shows O K-edge XAS spectra. The polymer solutions with high viscosity, required the use of custom-made cells for sealed measurements. The obtained results suggested characteristic changes on shake-gel at the pre-edge region. This suggests the characteristic hydration structure in the shake-gel.

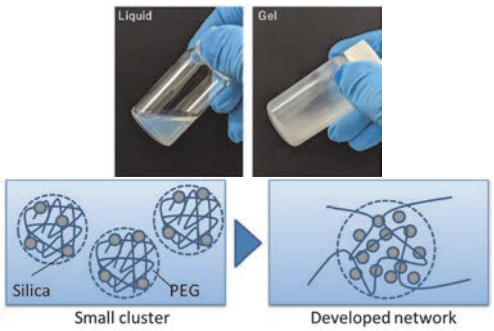


Fig. 1. Photo images of the shake-gel and schematic images of structural change of colloidal silica solution under dilatant phenomena.

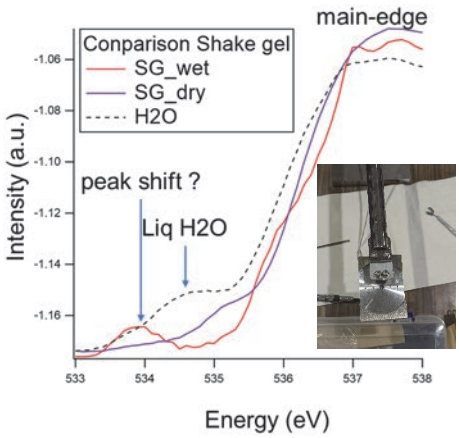


Fig. 2. XAS spectra of dry and wet shake-gel. Inset shows photo images of liquid cell.

[1] K. Akada *et al*., Colloids Surf. A **658** (2023) 130727.

BL3U

# Near-Edge X-ray Absorption Spectroscopy in a Ferroelectric Nematic Liquid Crystal

F. Araoka[1*], H. Nishikawa[1], Y. Takanishi[2] and H. Iwayama[3,4]
[1]*RIKEN Center for Emergent Matter Science (CEMS), Wako, Saitama 351-0198, Japan*
[2]*Department of Physics, Kyoto Prefectural University of Medicine, Sakyo, Kyoto 606-0823, Japan*
[3]*UVSOR Synchrotron Facility, Institute for Molecular Science, Okazaki, Aichi 444-8585, Japan*
[4]*School of Physical Sciences, The Graduate University for Advanced Studies (SOKENDAI), Okazaki, Aichi 444-8585, Japan*

Ferroelectric nematics (NF) are a new group of polar fluid liquid crystals (LCs) co-possessing liquid-like fluidity and ferroelectricity. Although such a polar order state was predicted by the well-known physicist, Max Born, in the early 20th century, it had not yet been realized until its discovery in 2017 by two independent groups [1,2]. Since then, it has attracted broad attention from the fundamental science to the potentials for novel applications. One of the most fascinating physical properties of NF is efficient generation of optical second harmonics, which is ~100 times larger than quartz, originating from efficient polar ordering in the present system. Recently, we reported cybotactic cluster formation stabilizing the NF phase in diastereomeric DIO mixtures [3]. In this case, anisotropy of the smectic clusters, estimated from small/wide angle X-ray analysis, clearly shows fatting of clusters as temperature decreases. This suggests a possibility that the side-by-side interaction may be an important role in stabilizing the polar ordering of the NF phase.

In this study, we performed near-edge X-ray absorption spectroscopy for the NF liquid crystal, DIO-C3 (Fig. 1). The carbon K-edge absorption spectrum was taken by scanning the photon energy of the soft X-ray irradiated on the sample sandwiched between two silicon nitride (SiN) membrane films (Fig. 2). The sample film was heated by a hot stage which equips input/output window to allow the X-ray beam to pass through. The transmitted X-ray was detected by a photodiode, and the generated photocurrent was recorded by a signal counter.

The obtained spectrum shows two signature peak regions (Fig. 3); one appearing in the lowest photon energy region (285~6 eV) is corresponding to the π-electrons in the molecule, the other in the higher energy region (above ~286.5eV) to the σ-electrons. Interestingly, the latter shows notable peak shift at the phase transition temperature from the N (SmZA) to NF phases, while the former shows only scarce change either in the peak position or shape. This means, the head-to-tail dipolar interaction, which affects the longitudinal σ-orbitals, is stronger than the effect of the side-by-side attraction contributed from the π-π interaction, in the present system. Thus, this is different from our expectation, described in the above introduction part. This was also discussed by comparing it with a theoretically computed near-edge X-ray absorption spectrum obtained with a density functional theory (DFT) calculation package for NEXAFS analysis. Further calculation and analysis are currently on-going.

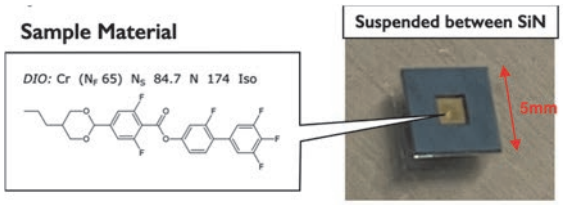


Fig. 1. Chemical structure of the NF molecule, DIO-C3 (Left), introduced between two SiN membrain films (Right).

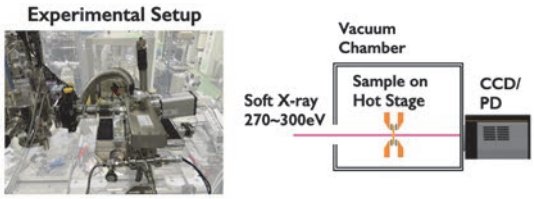


Fig. 2. Experimental setup prepared in the synchrotron soft X-ray at BL3U beamline of UVSOR, IMS, Japan.

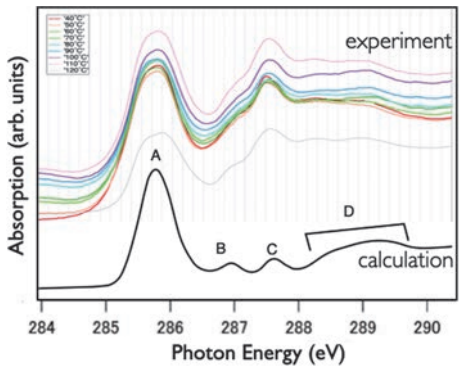


Fig. 2. Typical temperature-dependent absorption spectrum in the NF material, DIO-C3. The region A is corresponding to the π-orbital, and B, C and D are to the σ-orbitals of alkyls and dioxanes.

[1] H. Nishikawa *et al*., Adv. Mater. **29** (2017) 1702354.
[2] R. Mandle *et al*., Chem. Eur. J. **23** (2017) 14554.
[3] H. Nishikawa *et al*., Commun. Mater. **3** (2022) 89.

BL3U

# Oxygen K-Edge X-ray Absorption Spectroscopy for Identifying Active Surface Oxygen Species on Metal Oxide Catalysts

H. Tedzuka[1], N. Matsumoto[1], H. Saito[2], M. Nagasaka[3,4] T. Sugimoto[2,3] and Y. Sekine[1]
[1]*Department of Applied Chemistry, Waseda University, 3-4-1, Okubo, Shinjuku, Tokyo 169-8555, Japan*
[2]*Department of Materials Molecular Science, Institute for Molecular Science, Okazaki 444-8585, Japan*
[3]*Graduate University for Advanced Studies (SOKENDAI), Okazaki 444-8585, Japan*
[4]*UVSOR Synchrotron Facility, Institute for Molecular Science, Okazaki 444-8585, Japan*



Oxidative coupling of methane (OCM) is a single-step $C_2$ synthesis reaction from methane. In the field of heterogeneous catalysis, the investigation has been carried out for 50 years around the world [1]. However, high reaction temperature and low $C_2$ yield hinder the practical use of OCM. Recently, the first difficulty has been overcome by applying electric-field to the catalytic OCM reaction (EF-OCM). For instance, Sato et al. reported that the reaction temperature of OCM decreased from ~800 to 427 K in EF-OCM using Ca-doped $LaAlO_3$ catalysts [2]. The electric field contributes to generating active surface oxygen species, which are similar to those in thermal OCM [3], at low temperatures. Because there are various candidates for active surface oxygen species such as $O^{2-}$, $O^-$, $O_2^{2-}$, and $O_2^-$, identifying the active surface oxygen species is crucial for the rational design of high-performance EF-OCM catalysts. In this study, we conducted the O K-edge soft X-ray absorption spectroscopy for Ca-doped $LaAlO_3$ catalysts in the EF-OCM system.

The Ca-doped $LaAlO_3$ was prepared by a complex polymerization method from nitrate salts of La, Al and Ca as metal precursors [2]. The synthesized catalyst was milled and subsequently pressed to shape a wafer (10 mm in diameter and 1 mm thick). The shaped sample was set on a holder with three gold electrodes; the two electrodes were used for applying DC current and the other was employed for the total electron yield (TEY) measurement. The sample holder was inserted a chamber sealed with ConFlat flanges. EF-OCM was performed in the chamber filled with $CH_4/O_2$/He mixed reaction gas. Oxygen K-edge X-ray absorption spectra were recorded in TEY and total fluorescence (TFY) modes using a silicon drift detector.

Figure 1 shows the O K-edge spectra of 30%Ca-doped $LaAlO_3$ ($La_{0.7}Ca_{0.3}AlO_3$) recorded in the TFY mode. Before the reaction, two peak were observed at ~535 and ~542 eV, which are attributed to the electron transition from O1*s* to O2*p*-La5*d* and O2*p*-La6*sp* hybridized states, respectively [4]. After the reaction, a new peak was appeared in the pre-edge region at ~530 eV as shown by a yellow arrow in the dotted rectangle. This peak was remained after evacuating the chamber; the possibility of physisorbed $O_2$ is excluded. According to the literature, the observed peak at ~530 eV is attributable to the electron transition from O1*s* to O2*p*-Al3*p* hybridized state [4] or to the $O_2^-$ π* orbital [5]. Based on the assignment, we assume that applying the electric field would induce structural distortion of the Ca-doped $LaAlO_3$ catalyst or generate a new chemisorbed oxygen species. For the further identification, we plan to measure *operando* O K-edge spectra in several conditions and perform theoretical calculations. Although additional experiments and analyses are required to establish solid conclusions, we succeeded in obtaining an important clue to the reactive oxygen species in the EF-OCM system.

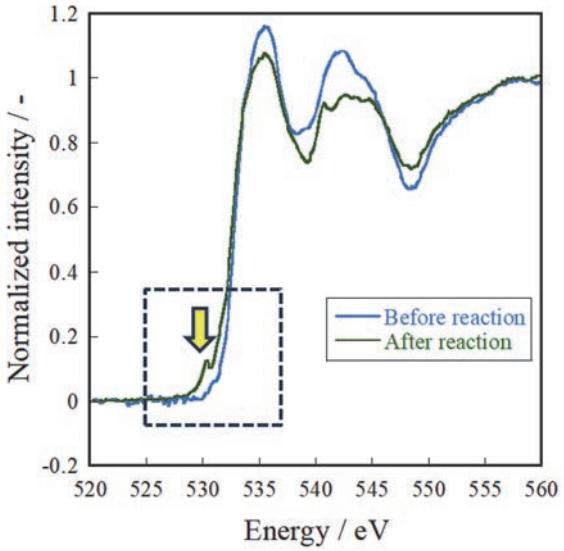


Fig. 1. O K-edge spectra of $La_{0.7}Ca_{0.3}AlO_3$ in TFY mode before and after EF-OCM reaction. These spectra were measured *in vacuo*.

[1] J.H. Lunsford, Angew. Chem. Int. Ed. **34** (1995) 970.
[2] A. Sato *et al*., ACS Omega **4** (2019) 10438.
[3] K. Sugiura *et al*., Sci. Rep. **6** (2014) 25154.
[4] N. Palina *et al*., Phys. Chem. Chem. Phys. **18** (2016) 13844.
[5] M.W. Ruckman *et al*., Phys. Rev. Lett. **67** (1991) 2533.

BL3U

# The Electronic States of 1-Methylimidazole in the Acetic Acid/1-Methylimidazole Mixture

Y. Horikawa[1], M. Okazaki[1] and M. Nagasaka[2]
[1]*Graduate School of Sciences and Technology for Innovation, Yamaguchi University, Yamaguchi 753-8512, Japan*
[2]*Institute for Molecular Science, Okazaki 444-8585, Japan*

Acetic acid (AcO) is a weak acid, so its degree of ionization is low, and the electrical conductivity of pure acetic acid is $3.8 \times 10^{-4}$ mS/cm. However, when acetic acid and 1-methylimidazole (1-MI, electric conductivity is $6.4 \times 10^{-2}$ mS/cm) are mixed, the electric conductivity of this solution increases to 8.0 mS/cm at concentrations of $\chi_{AcO} = 0.65$ and 0.85 (Fig. 1). We have applied soft X-ray emission spectroscopy to reveal the electronic states of acetic acid in the mixture at various mole fractions of acetic acid ($\chi_{AcA} = 0$~1) [2]. In the high concentration region of acetic acid ($\chi_{AcA}$ ~0.85) that exhibited high electrical conductivity, the amount of neutral acetic acid monomer in the mixture increased prior to an increase in the amount of acetate. On the other hand, in the concentration aroud $\chi_{AcA} \sim 0.7$ that also exhibited high electrical conductivity, the amount of acetate ions increased, indicating that the electrical conductivity increases as the number of ions increases. This was a natural phenomenon as it shows. From these two results, it was suggested that the electrical conduction mechanism is different in the two concentration ranges ($\chi_{AcA} = 0.7$ and 0.85). However, in the previous experiments [2], only acetic acid in the mixture was observed, so we needed to investigate how the number of ions in the solution was changing, and whether the ionization of 1-MI occurred along with the ionization of acetic acid. Therefore, we measured Nitrogen 1*s* X-ray absorption (XA) spectra of the mixture.

Figure 2 and 3 shows N 1*s* XA spectra of acetic acid/1-MI mixture and calculated XA spectra by using DFT calculations. In the measured spectra, it was observed that the first of the two resonance peaks seen in the pure 1-IM liquid disappeared as the acetic acid concentration increased. Furthermore, the calculation results in Fig. 3 show that when 1-MI is ionized, the first resonance peak shifts and is no longer observed. These results confirmed that 1-MI molecules become ionized at acetic acid molar concentrations around 0.7, and that most 1-MI exists in the form of ions in the high acetic acid concentration region. Considering this together with the results of the structural change of acetic acid, it can be concluded that the 1-MI is also fully ionized at an acetic acid mole fraction around 0.7, where acetic acid ions are at their maximum, and that at higher concentrations of acetic acid, the acetic acid monomer increases but requires the same amount of 1-MI ions as acetic acid ions, which are present in trace amounts, and that all molecules of 1-MI are considered ionized ($\chi_{AcA} = 0.8 \sim 0.9$). We plan to conduct detailed quantitative analysis.

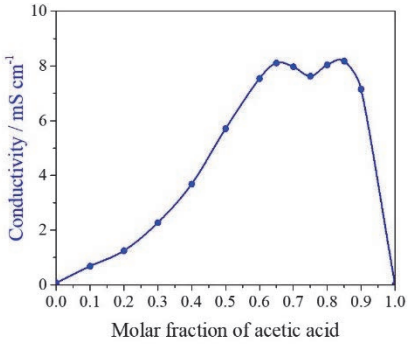


Fig. 1. Electrical conductivity of an acetic acid/1-MI mixture at various concentrations at ambient temperature [2].

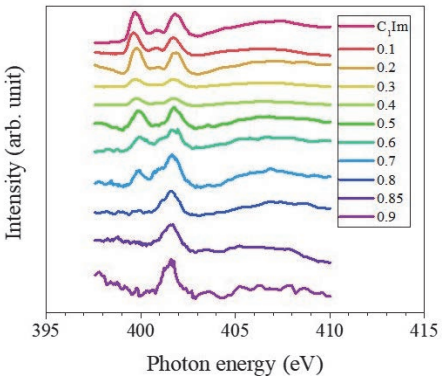


Fig. 2. N 1*s* XA spectra of acetic acid/1-MI mixture.

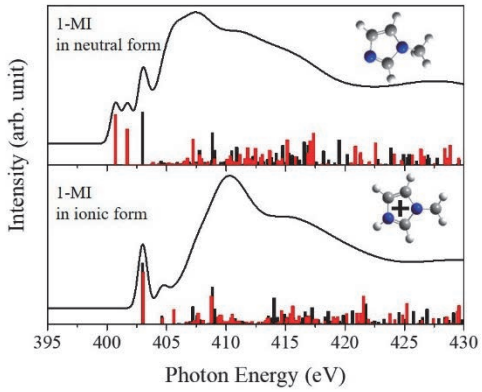


Fig. 3. Calculated N 1*s* XA spectra of acetic acid/1-MI mixture.

[1] H. Doi *et al*., Chem. Eur. J. **19** (2013) 11522.
[2] N. Yoshimura *et al*., J. Phys. Chem. B **123** (2019) 1332.

BL3U

# Soft X-ray Absorption of Semiconductor Photocatalyst Particles Suspended in Water

H. Onishi[1,2], Y. H. Chew[1], N. Ichikuni[3] and T. Yoshida[4]

[1]*Graduate School of Science, Kobe University, Kobe 657-8501, Japan*

[2]*Division of Advanced Molecular Science, Institute for Molecular Science, Okazaki 444-8585, Japan*

[3]*Graduate School of Engineering, Chiba University, Chiba 263-8522, Japan*

[4]*Reserch Center for Artificial Photosynthesis, Osaka Metropolitan University, Osaka 558-8585, Japan*



Material conversion on semiconductor photocatalysts is intensively studied worldwide. Downhill reactions, in which the Gibbs free energy decreases during the conversion of reactants to products, have been successfully integrated into our society [1]. Artificial photosynthesis, a category of uphill reactions involving the oxidation of water, is being developed for societal implementation in the near future [2]. In addition, fundamental studies are being conducted to uncover new scientific discoveries related to light-driven, efficient materials conversion [3].

Here, in collaboration with Prof. Masanari Nagasaka of UVSOR, we apply soft X-ray absorption to the *in-situ* characterization of semiconductor photocatalysts suspended in water. A representative photocatalyst, anatase $TiO_2$ (JRC-TIO-19 provided by Catalysis Society of Japan), was suspended in water. The suspended solution was adjusted with NaOH to pH 13. The pH adjustment was critical to suspend 100 nm $TiO_2$ particles long enough to pass through the liquid cell.

The liquid cell was mounted in BL3U. Oxygen K-edge and titanium L-edge absorption spectra were observed with a transmission setup [4] in the presence and absence of ultraviolet (UV) light for bandgap excitation.

Figure 1 shows the O K-edge and Ti L-edge spectra observed in the absence of UV light. In the O K-edge, electron transition from O1s to O2p orbitals of $TiO_2$ particles was detected at 530-533 eV together with intense absorption of water at 534 eV or higher energies. The O2p orbitals are hybridized with Ti3d orbitals to form the conduction band in $TiO_2$. The hybridized O2p orbitals are thus split into $t_{2g}$ and $e_g$ levels according to the ligand field in $TiO_6$ octahedra. Splitting into $t_{2g}$ and $e_g$ states also occurred in the Ti $L_3$- and $L_2$-edge absorption, respectively.

The soft X-ray absorption of solutions has been successfully studied. In this study, transmission measurement was achieved with a suspension. The extension to an *operando* study of the suspension under UV irradiation is promising.

This study was supported by JSPS KAKENHI (grant number 22H00344).

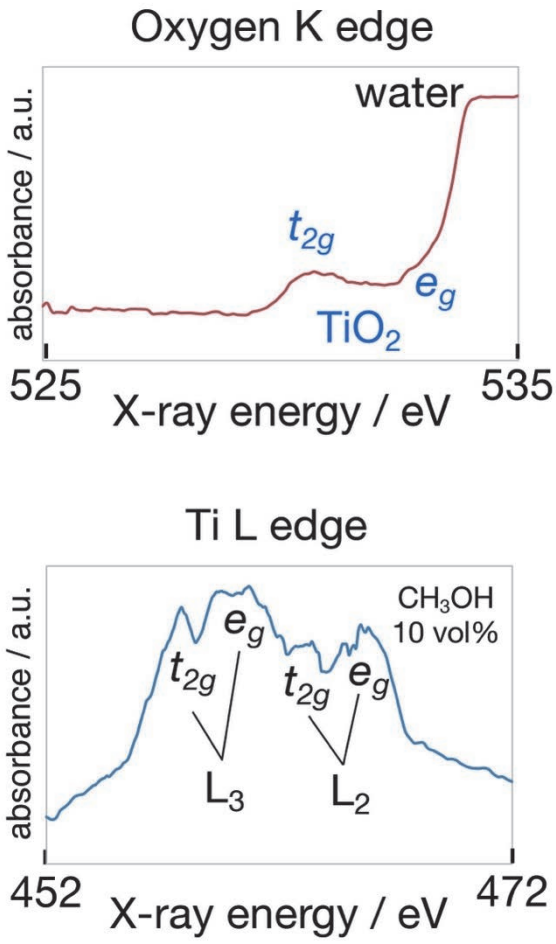


Fig. 1. Soft X-ray absorption of anatase $TiO_2$ photocatalyst particles (JRC-TIO-19) suspended in water at pH 13. Oxygen K-edge and titanium L-edge spectra were observed in the absence of UV light irradiation. Methanol (10 vol%) was added to the suspension for Ti L edge observation.

[1] A. Fujishima *et al.*, J. Photochem. Photobiol. C **1** (2000) 1.
[2] H. Onishi, ChemSusChem **12** (2019) 1825.
[3] C. Kranz and M. Wächtler, Chem. Soc. Rev. **50** (2021) 1407.
[4] T. Petit *et al.*, J. Phys. Chem. Lett. **6** (2015) 2909.

BL3U

# Probing the H-Bonding Network in the Vicinity of Aqueous Ammonia and Ammonium Ion by X-ray Absorption Spectroscopy

D. Céolin [1], T. Saisopa [2], Y. Rattanachai [2], W. Sailuam [3], H. Yuzawa [4] and N. Kosugi [4]

[1]*Synchrotron SOLEIL, l'Orme des Merisiers, Saint-Aubin, F-91192 Gif-sur-Yvette Cedex, France*

[2]*Department of Applied Physics, Faculty of Sciences and Liberal Arts, Rajamangala University of Technology Isan, Nakhon Ratchasima 30000, Thailand*

[3]*Department of Applied Physics, Faculty of Engineering, Rajamangala University of Technology Isan, Khon Kaen, Thailand*

[4]*UVSOR Synchrotron Facility, Institute for Molecular Science, Okazaki 444-8585, Japan*

Hydrogen bonds interaction has been largely probed in aqueous (aq) media by means of different experimental (FTIR, X-ray diffraction, emission and absorption) and theoretical (DFT, MP2, QM/MM) methods. Among these, X-ray absorption spectroscopy (XAS) is a very appropriate tool due to its sensitivity to local orders and geometrical changes around a selected center. In addition, monitoring the solution temperature was shown to be a good parameter to gain more insight into the interaction of, e.g., water with its surroundings [1]. Indeed, bulk water is sensitive to the temperature increase due to an increase of the distances between water molecules, leading to the weakening of the H-bond strength. Other systems presenting donating or accepting hydrogen bonds were also investigated, namely, ammonia and ammonium ion interaction with water were probed by XAS [2, 3] and FT-IR experiments [2]. It was concluded that $NH_3$(aq) has a medium strong hydrogen bond between its lone pair and a donating water molecule, whereas the donating character of the 3 N-H is considered as ultra-weak. In contrast, $NH_4^+$(aq) has 4 equivalent donating hydrogen bonds, all of them being in the weak category, weaker than the water-water bonding.

Based on these results, we performed temperature dependent XAS measurements at the BL3U beamline on ammonia and ammonium ion in aqueous solutions at the nitrogen K-edge. Measurements were done using the liquid cell of SiC membrane in transmission mode on solutions prepared at a concentration of 1 M. The normalized spectra are shown in the Fig. 1. For $NH_3$(aq), the spectrum presents an isolated pre-edge having a N2p character, followed by a sharp and intense double-structure main-edge and a long tail as a post-edge. The spectrum of $NH_4^+$(aq) starts at about 2 eV higher in energy, with the pre-edge that appears as a weak shoulder having a N2s character, on the low energy side of an intense main edge. It is followed by a less intense large shoulder as a post-edge.

The first original observation from this dataset is the splitting of the $NH_3$(aq) XAS main-edge leading to two maxima at 402.8 eV and 403.3 eV. In the gas phase, the main line is attributed the transition N1s to the doubly degenerated 2e orbitals [4]. This double structure, attributed to a degeneracy lift of the 2e orbital due to environment effects, was calculated but not clearly measured in reference [2]. The second observation concerns the intensity dependence of some structures with the temperature, for the two solutions. The spectra are compared in a way that the intensities on the low and high photon energy sides of the spectra are normalized to the same values for all temperatures. Following this procedure, we see that the temperature mostly influences the post-edge structures, as indicated by the arrows in the figures.

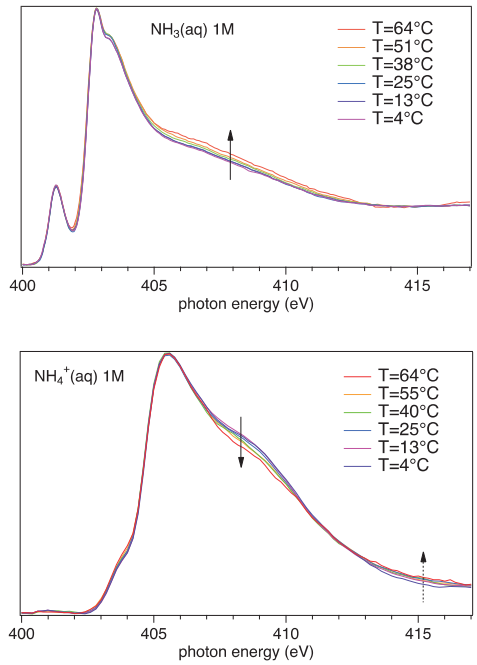


Fig. 1. X-ray absorption spectra of 1 M $NH_3$ (upper-panel) and $NH_4^+$ (lower-panel) aqueous solutions, recorded in the vicinity of the N1s ionization threshold, for temperatures in the 4-64 °C range.

[1] M. Nagasaka *et al.*, J. Phys. Chem. B **121** (2017) 10957.
[2] M. Ekimova *et al.*, J. Am. Chem. Soc. **139** (2017) 12773.
[3] P. Reinholdt *et al.*, J. Phys. Chem. Lett. **12** (2021) 8865.
[4] J. Schirmer *et al.*, Phys. Rev. A: At. Mol. Opt. Phys. **47** (1993) 1136.

BL3U

# Elucidation of Oxygen Evolution Reaction Mechanism on γ-$MnO_2$ Electrocatalyst during Electrolysis of Acidic Aqueous Solution by *Operando* Soft X-ray XAFS

A. Li[1], K. Adachi[2], D. Hashizume[2] and R. Nakamura[1,3]

[1]*Biofunctional Catalyst Research Team, RIKEN Center for Sustainable Resource Science (CSRS), Wako 351-0198, Japan*

[2]*Materials Characterization Support Team, RIKEN Center for Emergent Matter Science (CEMS), Wako 351-0198, Japan*

[3]*Earth-Life Science Institute (ELSI), Tokyo Institute of Technology, Meguro-ku 152-8550, Japan*

In the quest for sustainable energy solutions, electrochemical fuel synthesis powered by renewable resources stands out as a promising avenue to meet the world's growing energy demands [1]. Central to this endeavor is the conversion of water into fuel, a process that requires efficient catalysts to facilitate the electrochemical oxidation of water molecules. Transition metal oxides, particularly manganese oxides ($MnO_2$), have emerged as key contenders in this domain, offering a blend of advantages that make them attractive candidates for catalyzing water oxidation reactions.

Manganese-based catalysts hold significant appeal due to their lower toxicity and abundance compared to noble-metal-based counterparts like nickel, iron, or cobalt. While they may exhibit lower activity levels, their scalability and environmental friendliness make them an appealing choice for sustainable fuel synthesis. Drawing inspiration from biological catalysts, such as the $CaMn_4O_5$ cluster found in the Photosystem II enzyme [2], researchers have turned to $MnO_2$ as a potential solution for driving electrochemical water oxidation [3,4].

At UVSOR BL3U, we performed in-situ soft X-ray absorption measurements of the Mn L-edge for $Mn^{2+}$ ions in solution and electrodeposited $MnO_2$ (Figure 1). Pt/Cr/SiN film electrodes served as substrates. Even the water oxidation reaction on $MnO_2$ could not be achieved due to the instability of the deposited film on the Pt/Cr film and the formation of oxygen bubbles, we have obtained useful information of $Mn^{2+}$ and electrodeposited $MnO_2$ in 1 M $H_2SO_4$ solution. The thickness for Pt, Cr and SiN are 20 nm, 5 nm and 100 nm, respectively. Films of $MnO_2$ were deposited via oxidative electrodeposition at an applied potential of 1. 5 V on Au-coated SiN membranes from aqueous 0.36 M $Mn^{2+}$ solutions with 1 M $H_2SO_4$. Upon applying potential to initiate $MnO_2$ electrodeposition, a clear shift in the Mn L-edge absorption from $Mn^{2+}$ to $Mn^{3+/4+}$ was observed (Figure 1b). This shift indicates that electrodeposition occurred under electrochemical conditions, even in highly acidic environments (1 M $H_2SO_4$). For comparison, the Mn-K edge spectrum of $Mn^{2+}$ in 1 M $H_2SO_4$ was also measured (Figure 1a).

Despite the challenges encountered, our research successfully obtained the Mn L-edge XAS spectra of $Mn^{2+}$ and electrodeposited $MnO_2$ in harsh acidic condition.

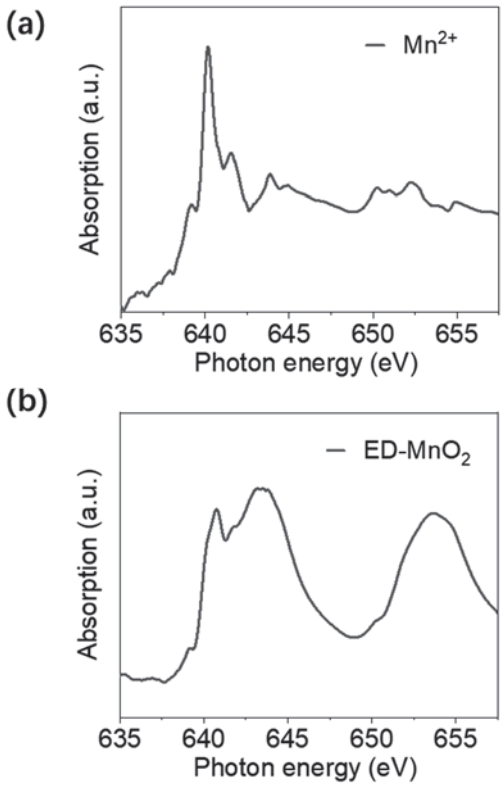


Fig. 1. Mn L-edge spectra of 0.35 M $Mn^{2+}$ and ED-$MnO_2$ in 1 M $H_2SO_4$.

[1] Chu, S. & Majumdar, Nature **488** (2012) 294.
[2] M. Suga *et al*., Nature **543** (2017) 131.
[3] A. Li *et al*., Angew. Chem. Int. Ed. **58** (2019) 5054.
[4] S. Kong *et al*., Nat. Catal. **7** (2024) 252.
[5] M. Nagasaka *et al*., J. Electron. Spectrosc. Relat. Phenom. **224** (2018) 93.

BL3U

# Isolated Water Molecules in Aqueous Acetonitrile Solutions Probed by Oxygen K-Edge X-ray Absorption Spectroscopy

M. Nagasaka[1,2]
[1]*Institute for Molecular Science, Okazaki 444-8585, Japan*
[2]*Graduate University for Advanced Studies, SOKENDAI, Okazaki 444-8585, Japan*

The properties of water molecules are changed from liquid phases to cluster structures due to the different hydrogen bond structures [1]. Since it is important to investigate the electronic structures of isolated water molecules, isolated water molecules were prepared by several techniques. On the other hand, water clusters are formed in aqueous acetonitrile solutions because it is inhomogeneous in a microscopic scale, which is known as microheterogeneity [2]. We have measured O K-edge X-ray absorption spectroscopy (XAS) of aqueous acetonitrile solutions and found a sharp peak profile around 537 eV, which would be derived from the confinement of water molecules with acetonitrile molecules by the dipole interactions [3]. The electronic structures of not only water clusters but also $H_3O^+$ clusters were also investigated by O K-edge XAS [4]. In this study, we investigated whether the sharp peak profiles in O K-edge XAS are derived from the completely isolated water molecules or small water clusters from the inner-shell calculations.

Figure 1(a) shows O K-edge XAS spectrum of aqueous acetonitrile solutions, $(ACN)_{0.9}(H_2O)_{0.1}$, obtained by our previous experiment [3]. The main-edge peak around 537 eV shows a shaper profile compared to liquid water and is close to that of water gas.

For investigating the relation of the sharp profiles of the main-edge peaks with the structures of water clusters, we have performed inner-shell calculations of small water clusters at different sizes. The structures of liquid water and small water clusters confined by acetonitrile were obtained by the molecular dynamics simulations. The inner-shell spectra of water clusters at different sizes were obtained by the summation of 14,900 spectra of water clusters extracted from the liquid structures with the simulation time of 100 ns, which include the deviation of the hydrogen bond structures [5].

Figure 1(b) shows O K-edge inner-shell spectra of liquid water and water clusters with the different sizes of 1 – 5. The second peak around 537 eV corresponds to the main-edge peak. The inner-shell spectra of water clusters with the sizes of 2 – 5 show nearly same spectral profiles and are close to those of liquid water. On the other hand, the inner-shell spectrum of water clusters with the size of 1, which are isolated water molecules, show different spectral profiles. It means that the sharp profiles of the main-edge peaks in O K-edge XAS of aqueous acetonitrile solutions derives not from small water clusters but from isolated water molecules surrounded by acetonitrile molecules.

The properties and dynamics of isolated water molecules has been previously investigated by the complicate manipulations such as the encapsulation of water molecules in fullerene or ionic liquids. This study found that isolated water molecules are easily formed in aqueous acetonitrile solutions at relatively high molar fraction of water because of the microheterogeneity. The electronic structures of isolated water molecules surrounded by acetonitrile molecules can be analyzed by the sharp profiles of the main-edge peak in O K-edge XAS spectra, separating the contributions of even small water clusters.

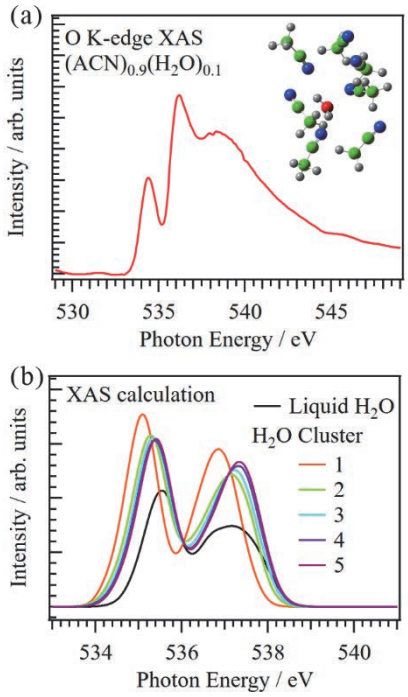


Fig. 1. (a) O K-edge XAS of aqueous acetonitrile solutions $(ACN)_{0.9}(H_2O)_{0.1}$. The inset shows isolated water molecules confined with acetonitrile. (b) O K-edge inner-shell spectra of liquid water and water clusters with different sizes in aqueous acetonitrile solutions.

[1] R. Ludwig, Angew. Chem. Int. Ed. **40** (2001) 1808.
[2] Y. Marcus, J. Phys. Org. Chem. **25** (2012) 1072.
[3] M. Nagasaka *et al.*, J. Phys. Chem. B **124** (2020) 1259.
[4] M. Ekimova *et al.*, Angew. Chem. Int. Ed. **61** (2022) e202211066.
[5] M. Nagasaka, J. Chem. Phys. **158** (2023) 024501.

BL3U

# Observation of Electrochemically Generated Reactive Intermediate for Methane Oxidation by Operando Electrochemical Soft X-ray Absorption Spectroscopy

Y. Yamada [1, 2] and M. Nagasaka[3]

[1]*Department of Chemistry, Graduate School of Science, Nagoya University, Furo-cho, Chikusa-ku, Nagoya 464-8602, Japan*

[2]*Research Center for Materials Science, Nagoya University, Furo-cho, Chikusa-ku, Nagoya 464-8602, Japan*

[3]*Institute for Molecular Science, Myodaiji, Okazaki 444-8585, Japan*

$CH_4$ is abundant in nature as natural gas or methane hydrate, whereas it is also recognized as an environmental pollutant having high greenhouse effect. Therefore, development of novel catalysts that convert $CH_4$ into valuable chemical feedstocks efficiently is highly desired. However, high chemical stability of C–H bonding of $CH_4$ makes it highly difficult. We recently reported that a μ-nitrido-bridged iron phthalocyanine dimer stacked on a graphite surface **1**/G (Fig. 1a) can activate C–H bonding of $CH_4$ efficiently and convert $CH_4$ into a mixture of methanol, formaldehyde, and formic acid in an acidic aqueous solution containing excess $H_2O_2$. The reactive intermediate is a high-valent iron-oxo species generated in situ (Fig. 1a). The catalytic C–H bond activation activity of $CH_4$ by **1**/G is quite high among a variety of molecule-based $CH_4$ oxidation catalysts and even comparable to that of a natural particulate methane monooxgenase (pMMO)[1].

We are now attempting to develop the method for electrochemical generation of $\mathbf{1}_{oxo}$/G without using $H_2O_2$ as an oxidant. We hypothesized that $\mathbf{1}_{oxo}$/G could be generated through the reaction shown in Fig. 1b, where electrochemical oxidation of coordinating $H_2O$ on the iron center of **1**($H_2O$)/G afford $\mathbf{1}_{oxo}$/G. Actually, in our previous experiment, we could successfully observe the peak corresponding to the O1s – π* of Fe=O for $\mathbf{1}_{oxo}$ by applying 1.8 V vs. Ag/AgCl to **1**($H_2O$)/G in a buffer solution (pH 7.0) by operando soft X-ray spectroscopy in UVSOR BL 3U.

Herein, we attempted to observe the peak corresponding to the O1s – π* of Fe=O for $\mathbf{1}_{oxo}$ by changing the applied voltage. A SiN membrane tip coated with carbon membrane (20 nm thickness), on which **1**($H_2O$) was stacked, **1**($H_2O$)/cmSiN (Fig. 2a) was used for this purpose. Electrochemical oxidation of **1**($H_2O$)/cmSiN was monitored by observing the O K-edge XAS spectra in a 100 mM phosphate buffer (pH = 7.0) by using a beamline equipped with a transmission-type liquid flow cell in BL3U of UVSOR [2]. The measurements were performed by changing the applied voltage to **1**($H_2O$)/cmSiN in a buffer solution and the spectra were obtained based on the Lambert-Beer law, $\ln(I_0/I)$, where $I_0$ is the transmission signals of the cmSiN in buffer and $I$ is those of **1**($H_2O$)/cmSiN at different applied voltage.

The obtained spectra were shown in Fig. 2b. The broad peak at around 532 eV was gradually increased after increasing the applied voltage from 0.70 V to 1.60 V vs. SHE (Fig. 2b). DFT calculation suggested that the peak of O1s – π* of Fe=O for $\mathbf{1}_{oxo}$ should be observed at around 529 eV, whereas the peaks for a coordinating $H_2O$ on iron ion of **1** should be observed at higher energy than 534 eV. Taking these results, the peak appeared at around 532 eV is assignable to the excitation of O1s – π* of Fe=O of electrochemically generated high-valent iron-oxo species of **1**($H_2O$)/cmSiN ($\mathbf{1}_{oxo}$/cmSiN). It was demonstrated that the high-valent iron-oxo species was generated after applying 1.30 V vs. SHE.

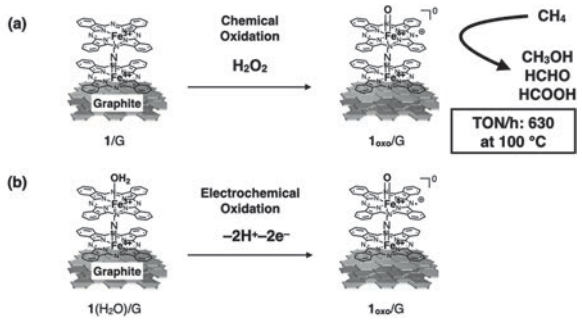


Fig. 1. Generation of $\mathbf{1}_{oxo}$/G from **1**/G by (a) treatment with $H_2O_2$ or (b) electrochemical oxidation.

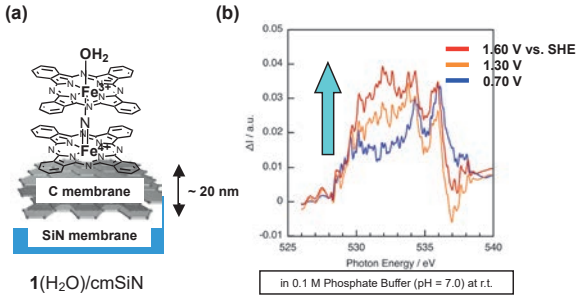


Fig. 2. (a) Structure of **1**($H_2O$)/cmSiN. (b) Comparison of O K-edge XAS spectra of **1**($H_2O$)/cmSiN after applying the indicated voltages vs. SHE in a phosphate buffer (pH = 7.0).

[1] Y. Yamada *et al.*, JACS Au. **3** (2023) 823.
[2] M. Nagasaka and N, Kosugi, Chem. Lett. **50** (2021) 956.

BL3B

# Photoelectron–Photoion Coincidence (PEPICO) for Hydrofluoroethanes

T. T. Nguyen [1], K. Ishikawa[1], T. Hayashi[1],
S. N. Hsiao[1] and H. Iwayama[2]
[1]*Center for lowtemperature plasma sciences,Nagoya University, Nagoya 464-8601, Japan*
[2]*UVSOR Synchrotron Facility, Institute for Molecular Science, Okazaki 444-8585, Japan*

Molecular ionization and dissociation processes of perfluorocarbons (PFCs) and hydrofluorocarbons (HFCs) in plasma etching chemistry are essential for determining of the plasma etching performance of dielectrics, such as $SiO_2$, SiN, in advanced semiconductor device fabrications. Desirable characteristics, such as fast etch rates and high etch selectivity should be achieved by counterbalancing between undesirable deposition of polymeric films onto the substrate and energic removal of underlying materials. A control of both the composition and the amount of ions and radical species generated from the source gas is a critical problem of the etching process. In this study, we have investigated about the primary dissociation pathways of PFCs and HFCs through a combination of experiments and calculations.

Prediction of the dissociation and ionization pathways for hydrofluorocarbonethanes was performed by using the computational chemistry technique. As a result, the electronic properties and primary dissociation channels of fluoroethane compounds from computational chemistry was reported, as listed in Table 1 [1]. The reactive ion etching performances of films of poly-Si, $SiO_2$ and SiN were also reported previously [2]. To verify experimentally the computational prediction, this study has conducted the photoelectron-photoion coincidence (PEPICO) experiments, for evaluation of the vacuum ultraviolet (VUV) light-induced decomposition of fluoroethane compounds.

The PEPICO measurements were performed in the BL3B in the UVSOR facility. Gases ($C_2H_xF_{6-x}$) introduced into a vacuum chamber and were kept less than $3\times10^{-4}$ Pa. The gases were irradiated by vacuum ultraviolet light energy from 10 to 28 eV (wavelength of 40-730 nm) in each 0.02 eV steps, with a spherical grating with grooves of 1200 l/mm. The ionized molecular fragments were detected by a time-of-flight (TOF) mass spectrometer. Appearance energies (AE) were determined by linearly extrapolating the threshold photon energy in which the ion yield became zero.

The photoionization of $CH_2FCHF_2$ (HFC143) was measured by the TOF mass spectra. The parent ion and its fragments, such as $CHF_2^+$, $CH_2F^+$, $CFCH_2^+$, and $CHFCH_2F^+$ were analyzed. The PEPICO results gave AE of 12.5 eV for $CHF_2^+$ and this was also found to be the dominant ion fragment (Figure 1). These results agree with previously calculated values [1], as compared with the results of $C_2F_6$ (PFC116).

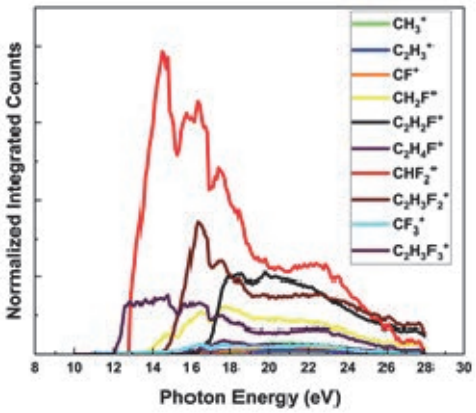


Fig. 1. Ion yield curves for photo-ionization.

Table 1. The primary dissociated ions and radicals[1].

| Molecules | Ions | Radical | Negative ions |
|---|---|---|---|
| $C_2H_5F$ | $CH_2F^+$, $C_2H_4F^+$, $C_2H_5^+$ | $C_2H_5$, $CH_3$, $CH_2F$ | $F^-$ |
| $CH_3CHF_2$ | $CHF_2^+$, $C_2H_3F_2^+$, $C_2H_4F^+$ | $C_2H_4F$, $CH_3$, $CHF_2$ | $F^-$, $C_2H_3F_2^-$ |
| $CH_2FCH_2F$ | $C_2H_4F_2^+$, $CH_2F^+$, $C_2H_4F^+$, $C_2H_3F_2^+$ | $CH_2F$, $C_2H_4F$ | $F^-$ |
| $CH_2FCHF_2$ | $CH_2F^+$, $CHF_2^+$, $C_2H_3F_2^+$, $C_2H_2F^+$ | $C_2H_3F_2$, $CH_2F$, $CHF_2$ | $F^-$ |
| $CH_3CF_3$ | $CH_3^+$, $C_2H_3F_2^+$, $CF_3^+$ | $CH_3$, $CF_3$, $C_2H_3F_2$ | $F^-$, $CH_2CF_3^-$ |
| $CHF_2CHF_2$ | $CHF_2^+$, $C_2H_2F_3^+$ | $CHF_2$, $C_2H_2F_3$, $C_2HF_4$ | $F^-$ |
| $CH_2FCF_3$ | $CF_3CH_2^+$, $CF_3^+$, $CH_2F^+$ | $CF_3$, $CH_2F$ | $F^-$, $CF_3^-$ |
| $CHF_2CF_3$ | $C_2HF_4^+$, $CF_3^+$, $CHF_2^+$ | $CF_3$, $CHF_2$ | $F^-$, $CF_3^-$ |
| $C_2F_6$ | $C_2F_5^+$, $CF_3^+$ | $CF_3$ | $F^-$, $CF_3^-$ |

[1] T. Hayashi *et al*. Jpn. J. Appl. Phys. **58** (2019) SEEF01.
[2] S-N. Hsiao *et al*.: Appl. Surf. Sci. **541** (2021) 148439.

BL4B

# Fragmentation of $OCS^{3+}$ States Studied by Multi-Electron–Ion Coincidence Spectroscopy

Y. Hikosaka

*Institute of Liberal Arts and Sciences, University of Toyama, Toyama 930-0194, Japan*

Significant experimental effort has been devoted to understanding the dissociation pathways and mechanism of triply charged ion states in carbonyl sulfide. Information on the $OCS^{3+}$ electronic states relevant to the dissociation pathways is, however, very limited, because it requires a spectroscopic method that relates the kinetic energies of multiple electrons ejected in the formation of $OCS^{3+}$ states to the ion species produced. In this study, the dissociation processes of the $OCS^{3+}$ states populated by the S 2p double Auger decay of OCS were investigated by multi-electron–ion coincidence spectroscopy [1]. A magnetic bottle electron spectrometer with ion detection capability [2-5] was employed for this measurement, and the high detection efficiencies for electrons enabled us to derive information on the fragmentations of $OCS^{3+}$ states.

The formation of $OCS^{3+}$ states by the S2p double Auger decay can be isolated by the electron triple coincidence of S 2p photoelectron and the associated two Auger electrons. Figure 1(a) shows the histogram of the energy sum of the two Auger electrons detected in coincidence with a S 2p photoelectron, displaying the $OCS^{3+}$ spectrum populated by the double Auger decay. Several peaks are observed in the kinetic energy range of 95-115 eV, and their main contributors are indicated in the figure. Moreover, a broad structure is seen in the binding energy range of 80-95 eV, resulting from densely lying excited states, most of which probably have holes in an inner-valence orbital.

The fragmentation of these $OCS^{3+}$ states can be investigated by inspecting the ion species detected in further coincidence. The two-dimensional map in Fig. 1(b) shows the correlations between the $OCS^{3+}$ spectrum and the times-of-flight of ions, derived from four-fold coincidences of three electrons and an ion. One finds on the two-dimensional map that horizontal stripes associated with different ion species show different $OCS^{3+}$ distributions. The $OCS^{3+}$ spectra in coincidence with individual ions, corresponding to the lineouts of the horizontal stripes on the map, are presented in Fig. 2. The $OCS^{3+}$ spectra coincident with molecular fragments $CO^+$ and $CO^{2+}$ exhibit $OCS^{3+}$ states relevant to the two-body dissociations into the $CO^+ + S^{2+}$ and $CO^{2+} + S+$ pairs, respectively. Though atomic fragments $C^+$ and $O^+/S^{2+}$ are not associated with a single dissociation channel, the corresponding coincidence spectra relevant to the three-body dissociation channels of $O^+ + C^+ + S^+$, $O + C^+ + S^{2+}$, and $O^+ + C + S^{2+}$. A detailed discussion of the fragmentations of individual $OCS^{3+}$ states is given in [1].

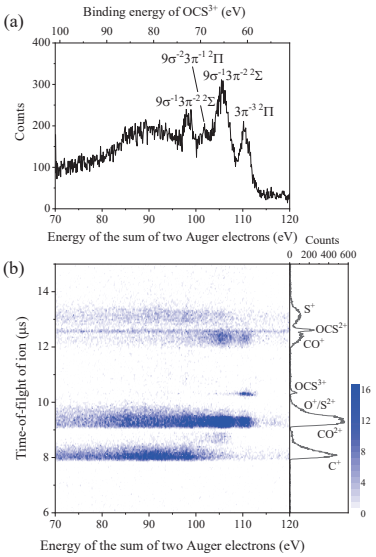


Fig. 1. (a) Spectrum for $OCS^{3+}$ formed by the S 2p double Auger decay. (b) Correlation map between the $OCS^{3+}$ states and ion times-of-flight in the right panel.

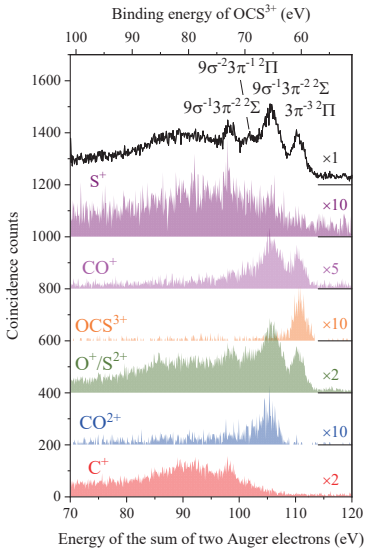


Fig. 2. Spectra of the $OCS^{3+}$ states filtered by coincidence with product ions.

[1] Y. Hikosaka, J. Chem. Phys. **158** (2023) 214306.
[2] Y. Hikosaka and E. Shigemasa, Int. J. Mass Spectrom. **439** (2019) 13.
[3] Y, Hikosaka, J. Electron. Spectrosc. Relat. Phenom. **255** (2022) 147158.
[4] Y. Hikosaka and S. Fritzsche, Phys. Chem. Chem. Phys. **24** (2022) 17535.
[5] Y, Hikosaka, Phys. Rev. A: At. Mol. Opt. Phys. **106** (2022) 062814.

BL4B

# Dissociation of Doubly Charged Ion States in Xenon Difluoride Molecules

Y. Hikosaka

*Institute of Liberal Arts and Sciences, University of Toyama, Toyama 930-0194, Japan*

Xenon difluoride ($XeF_2$) is a unique triatomic molecule constructed by weak bonding between the central rare-gas atom and fluorine ligands. The Auger decay of the core hole formed in the central Xe is of particular interest in terms of how the molecular environment affects the process. In addition, the stability and dissociation of the $XeF_2^{2+}$ states produced by the Auger decay remain unclear. In this study, the stability and dissociation processes of the $XeF_2^{2+}$ states produced by the Auger decay from the 4d core-hole formed in the central Xe atom were studied by multi-electron–ion coincidence spectroscopy [1] using a magnetic bottle electron spectrometer with ion detection capability [2-5].

The top panel of Fig. 1 shows the 4d photoelectron spectrum measured for a gas mixture of $XeF_2$ and Xe. The $4d^{-1}$ spin–orbit levels in $XeF_2$ shift to a higher binding energy of approximately 1.5 eV compared with the corresponding levels in Xe. The two-dimensional map in Fig. 1 displays the energy correlations of these 4d photoelectrons and the associated Auger electrons. The vertical stripes on the map are formed by the Auger electrons emitted from individual core-hole states. The Auger spectra associated with the $4d_{5/2}$ and $4d_{3/2}$ core-hole states of $XeF_2$ are derived by projecting the coincidence yields along the corresponding vertical stripes toward the vertical axis of the map and are shown in the right panel of Fig. 1. Here, the contamination from the Auger decay of Xe was subtracted.

The fragmentation of the Auger-final $XeF_2^{2+}$ states can be revealed by ion species detected in further coincidence. The two-dimensional map in Fig. 2 shows the correlations between the $XeF_2$ $4d_{3/2}$ Auger spectrum and the times-of-flight of product ions. The distributions of the $XeF_2^{2+}$ states relevant to individual ion formations are shown as horizontal stripes on the map, which drastically differ according to the ion species. One interesting observation is that coincidences with parent $XeF_2^{2+}$ ion are visible, revealing that part of the $XeF_2^{2+}$ states survived in the 10-μs time regime by overcoming the Coulomb repulsion between the two positive charges. It is found that the formation of the metastable $XeF_2^{2+}$ ion is associated with the state around a binding energy of 32 eV, which can be the ground $XeF_2^{2+}$ state with the configuration of $5\pi_u^{-2}$. On the other hand, other excited $XeF_2^{2+}$ states are all dissociative, and various dissociation fragments are formed. A detailed discussion of dissociations of individual $XeF_2^{2+}$ states is given in [1].

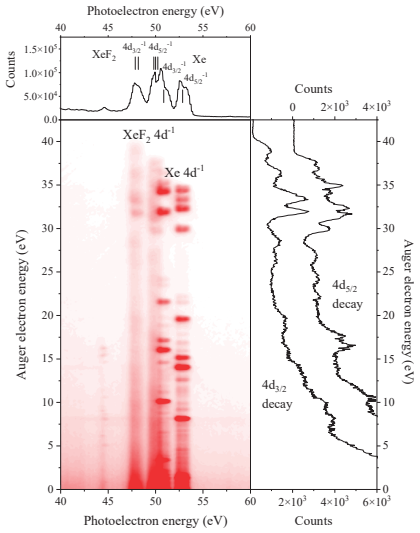


Fig. 1. Two-dimensional map of the energy correlation between the Xe 4d photoelectron and Auger electrons emitted from the gas sample of a mixture of $XeF_2$ and Xe at a photon energy of 120.4 eV.

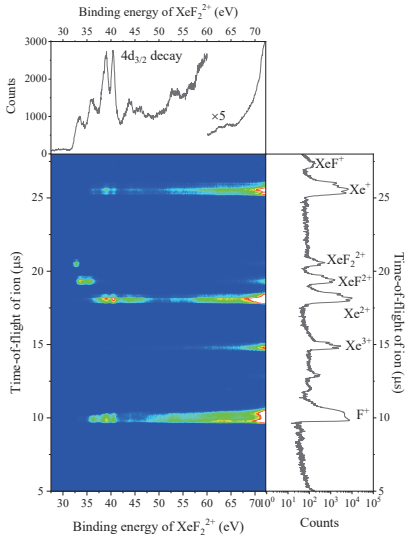


Fig. 2. Two-dimensional map of the correlation between the $XeF_2^{2+}$ states (top) and times-of-flight of ions (right).

[1] Y. Hikosaka, J. Chem. Phys. **160** (2024) 024304.
[2] Y. Hikosaka and E. Shigemasa, Int. J. Mass Spectrom. **439** (2019) 13.
[3] Y, Hikosaka, J. Electron. Spectrosc. Relat. Phenom. **255** (2022) 147158.
[4] Y. Hikosaka and S. Fritzsche, Phys. Chem. Chem. Phys. **24** (2022) 17535.
[5] Y, Hikosaka, Phys. Rev. A: At. Mol. Opt. Phys. **106** (2022) 062814.

BL7B

# High-Resolution Photoelectron Spectroscopy of Substituted Oxiranes

H. Kohguchi[1], Y. Hikosaka[2], T. Kaneyasu[3], S. Wada[1] and Y-I. Suzuki[4]
[1]*Graduate School of Advanced Science and Engineering, Hiroshima University, Higashi-Hiroshima 739-8526, Japan*
[2]*Institute of Liberal Arts and Sciences, University of Toyama, Toyama 930-0194, Japan*
[3]*SAGA Light Source, Tosu 841-0005, Japan*
[4]*School of Medical Technology, Health Sciences University of Hokkaido, Tobetsu 061-0293, Japan*



The substituent effect of organic molecules on photoelectron spectroscopy has been studied for a long time. The alkyl group is considered to only moderately modify the photoelectron spectral peak structures unless the relevant molecular orbitals are located closely to the substitution group. We conducted the measurements of the photoelectron spectra of oxiranes with different alkyl substituents at BL7B. Velocity-mapping imaging (VMI) was employed for obtaining the photoelectron spectra since the scattering distributions of these oxiranes are of our interest [1]. The photoelectron kinetic energy also modifies the photoelectron spectra, whose band intensity is subject to the photoionization dynamics [2]. The spectral resolution with the VMI-base measurement is not expected to be higher than the conventional UPS method, on which we relied as a reference for the spectral assignments at a standard photon energy (55 nm).

We measured the photoelectron images of oxirane derivatives at several photon energies from the ionization threshold to 55 nm. The photoelectron spectrum measured at 55 nm photon energy can be directly compared with previous data in the literature. Oxiranes are liquid samples at room temperature with sufficiently high vapor pressure to generate the effusive beam of oxiranes introduced into the VMI vacuum chamber. Observed photoelectron spectra of methyl oxirane at several photon energies are shown in Figure 1. These spectra were obtained by integrating the photoelectron signals of the observed image data for whole scattering angles. The kinetic energy (and the ionization potential) were calibrated with the VMI image data of He at the corresponding photon energies. The ionization potential of methyl oxirane (10.26 eV) was well reproduced in the present measurements, indicating good accuracy of our data.

Most of the observed band peaks (Fig. 1) were assignable in comparison with the photoelectron spectra in the literature. However, we found the following new features in the experimental results: (i) the relative intensity of the assigned peaks to certain ionic states was varied with the photon energy, (ii) the band intensity measured at 55 nm photon energy, which should be identical to the literature data, was different from the previous data with conventional UPS method. (iii) several band peaks were detected as a shoulder feature in the main bands for the first time. The detailed analysis of these experimental results should reveal unexplored photoionization dynamics of methyl oxirane.

We extended the measurements and analysis to oxirane derivatives in the same manner. While substituting the methyl group to the larger alkyl group yielded a quite similar photoelectron spectrum to that of methyl oxirane, a remarkably different spectrum was obtained for an aromatic derivative. The substation effect is mostly explained as the different interaction strengths between the oxirane framework and the substituents. However, newly found peaks for methyl oxirane (iii) were also observed for alkyl- and aromatic-oxiranes as shoulder-type features associated with the prominent bands. Further investigation of the observed spectra of oxirane-derivative is undertaken with quantum chemistry calculations.

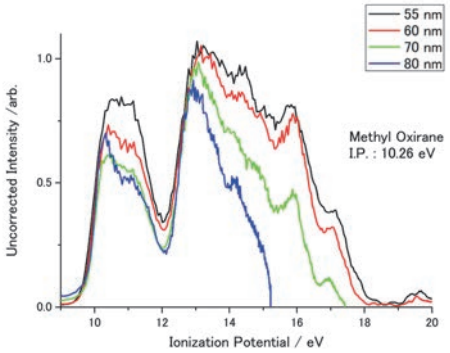


Fig. 1. Photoelectron spectra of methyl oxirane at several photon energies. The ionization threshold is identical with the literature value within the instrumental resolution.

[1] H. Kohguchi *et al.*, UVSOR Activity Report **50** (2023) 121.
[2] H. Kohguchi *et al.*, UVSOR Activity Report **48** (2021) 93.

BL7B

# Photoionization Experiments in UVSOR-III for Study of Divertor Plasmas in a Nuclear Fusion Reactor and of Interstellar Plasmas in a Context of Astrobiology

M. Kobayashi[1], S. Yoshimura[1], J. Takahashi[2], H. Iwayama[3], N. Kondo[3], M. Katoh[3,4], K. Kobayashi[5] and H. Nakamura[1]

[1]*National Institute for Fusion Science, Toki 509-5292, Japan*
[2]*Self-organization Science Research Center, Doshisha University, Kyotanabe 610-0321, Japan*
[3]*UVSOR Synchrotron Facility, Institute for Molecular Science, Okazaki 444-8585, Japan*
[4]*Hiroshima Synchrotron Radiation Center, Hiroshima University, Higashi-Hiroshima 739-0046, Japan*
[5]*Department of Earth and Planetary Sciences, Tokyo Institute of Technology, Meguro-ku, Tokyo 152-8550 Japan*

In nuclear fusion reactors, density of plasmas and neutral hydrogen in the divertor region will increase by more than one order of magnitude compared to the present-day devices due to the increasing plasma pressure in the scrape-off layer (SOL) [1]. At the same time, the photon emission from plasmas in confinement region (Bremsstrahlung) and in the SOL (line emissions from highly charged ions) will increase in wide wavelength range, from EUV to visible and infrared regions, because of the higher plasma density required to sustain nuclear fusion reaction. Such situation leads to enhanced interaction between hydrogen atoms/molecules and the photons in the divertor region, such as photoionization, photoexcitation. The atomic/molecular processes will be altered under the influence of the increased numbers of photons especially in very low temperature range below ~10 eV [2, 3].

There exist partially ionized plasmas in an interstellar space, where ionization is caused by cosmic rays or by interstellar radiation field [4]. In this circumstance, photon-induced processes, such as photoionization, photoexcitation, photodissociation etc., also play important roles in chemical evolution of prebiotic molecules related to the origin of life in space [5]. It is also noted that collective phenomenon of plasmas under the effects of magnetic fields will provide additional effects on the evolution. Characteristics and roles of the photoionized plasmas are, however, not yet fully understood.

To address these issues, we attempt to generate photoionized plasmas by using the synchrotron radiation source UVSOR-III [6] to simulate the above mentioned plasmas in the divertor region in nuclear fusion reactors and in the interstellar space. The beamline BL7B is used to generate beam from 30 to 500 nm. A gas cell has been installed inside the irradiation chamber to maintain high pressure of sample gas while keeping a good vacuum condition for the beamline. A high gas pressure is necessary to enhance the photoionization events through an interaction between the photons and neutral atoms/molecules. Fig.1 shows the gas cell used in the present experiments. The beam from BL7B is injected to the cell through a hole at the front end (ϕ 2 mm and 60 mm length). The beam is damped at the end of the gas cell. An off-axis parabolic mirror is installed at the front end to collect emission from the gas along the beam axis. An electrode of Langmuir probe is situated at the center of the cell and biased to +/- 18 V to measure saturation current of the plasmas. The gas is fed to the cell through the input terminal at the top of the cell.

As a sample gas, Argon (ionization potential of 14.5 eV) was introduced. The gas pressure inside the gas cell could be increased to an order of 1 Pa while the ambient pressure outside of the cell was kept at an order of $10^{-4}$ Pa and the pressure at the upstream of the beamline was at an order of $10^{-6}$ Pa. The photon flux of the beam was measured with a photodiode, and was estimated at an order of $10^{15} \sim 10^{16}$ photons/s/mm$^2$. The estimated electron density obtained by the Langmuir probe is in an order of $10^{11}$ m$^{-3}$, which is in agreement with a simple 1D model of the photoionization plasmas.

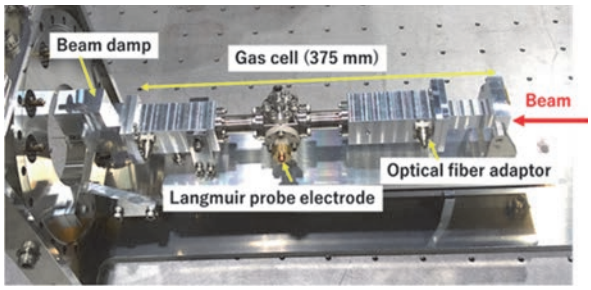


Fig. 1. Photo of the gas cell for photoionization experiments.

[1] M. Kotschenreuther *et al*., Phys. Plasma **14** (2007) 072502.
[2] K. Sawada *et al*., Contrib. Plasma Phys. **60** (2020) e201900153.
[3] M. Kobayashi *et al*., Contrib. Plasma Phys. **60** (2020) e201900138.
[4] E.F.van Dishoeck *et al*., Faraday Discuss. **133** (2006) 231.
[5] K. Kobayashi *et al*., Astrobiology **21** (2021) 1479.
[6] H. Ota *et al*., J. Phys. Conf. Ser. **2380** (2023) 012003.

# UVSOR User 5